Acta Crystallographica Section D
Biological Crystallography
ISSN 0907-4449

The 1.2 Å resolution crystal structure of TcpG, the *Vibrio cholerae* DsbA disulfide-forming protein required for pilus and cholera-toxin production

Patricia M. Walden,[a] Begoña Heras,[a]‡ Kai-En Chen,[a]§ Maria A. Halili,[a] Kieran Rimmer,[b] Pooja Sharma,[b]¶ Martin J. Scanlon[b] and Jennifer L. Martin[a]*

[a]Division of Chemistry and Structural Biology, Institute for Molecular Bioscience, University of Queensland, Brisbane, Queensland 4072, Australia, and [b]Medicinal Chemistry, Monash Institute of Pharmaceutical Sciences, Monash University, 381 Royal Parade, Parkville, Victoria 3052, Australia

‡ Current address: Latrobe Institute for Molecular Sciences, Latrobe University, Bundoora, Victoria, Australia.
§ Current address: Academia Sinica, Taipei, Taiwan.
¶ Current address: Walter and Eliza Hall Institute, Parkville, Victoria, Australia.

Correspondence e-mail: j.martin@imb.uq.edu.au

Received 10 March 2012
Accepted 11 June 2012

PDB Reference: TcpG, 4dvc.

The enzyme TcpG is a periplasmic protein produced by the Gram-negative pathogen *Vibrio cholerae*. TcpG is essential for the production of ToxR-regulated proteins, including virulence-factor pilus proteins and cholera toxin, and is therefore a target for the development of a new class of anti-virulence drugs. Here, the 1.2 Å resolution crystal structure of TcpG is reported using a cryocooled crystal. This structure is compared with a previous crystal structure determined at 2.1 Å resolution from data measured at room temperature. The new crystal structure is the first DsbA crystal structure to be solved at a sufficiently high resolution to allow the inclusion of refined H atoms in the model. The redox properties of TcpG are also reported, allowing comparison of its oxidoreductase activity with those of other DSB proteins. One of the defining features of the *Escherichia coli* DsbA enzyme is its destabilizing disulfide, and this is also present in TcpG. The data presented here provide new insights into the structure and redox properties of this enzyme, showing that the binding mode identified between *E. coli* DsbB and DsbA is likely to be conserved in TcpG and that the $\beta5$–$\alpha7$ loop near the proposed DsbB binding site is flexible, and suggesting that the tense oxidized conformation of TcpG may be the consequence of a short contact at the active site that is induced by disulfide formation and is relieved by reduction.

1. Introduction

The Gram-negative pathogen *Vibrio cholerae* is the causative agent of cholera, a serious acute infection of the small intestine caused by the ingestion of contaminated food or water. Central to the pathogenicity of *V. cholerae* is the production of a colonization pilus known as the toxin-coregulated pilus (TCP) that facilitates the adherence of *V. cholerae* to host microvilli (Peterson, 2002). The *V. cholerae tcpa* gene encodes a major subunit of TCP (Chakraborty *et al.*, 2000) and the *tcpg* gene encodes a protein essential for maturation and function of TCP proteins (Peek & Taylor, 1992). The gene product TcpG is a thioredoxin-fold redox enzyme that catalyzes the oxidative folding of several *V. cholerae* virulence factors, including cholera toxin, and has been identified as a potential target for the development of antibacterial compounds (Peek & Taylor, 1992; Heras *et al.*, 2009; Hu *et al.*, 1997).

TcpG shares 40% sequence identity with the *Escherichia coli* enzyme DsbA (EcDsbA). Like TcpG, EcDsbA is essential for the correct folding of secreted disulfide-containing bacterial proteins (Bardwell *et al.*, 1991), including many virulence factors (reviewed in Heras *et al.*, 2009). The redox properties of EcDsbA have been well characterized: it slowly reduces the intermolecular disulfide bond of insulin in the

classic insulin-reduction assay (Bardwell *et al.*, 1993), it is a strong oxidant (redox potential −122 mV at pH 7.0; Huber-Wunderlich & Glockshuber, 1998) and it is re-oxidized by its partner protein *E. coli* DsbB and cofactor ubiquinone (UQ1) in the bacterial inner membrane (Bardwell *et al.*, 1993; Inaba & Ito, 2002). The crystal structure of EcDsbA (Martin *et al.*, 1993) comprises a thioredoxin fold (Martin, 1995) with an inserted helical domain. An active-site C*XX*C motif that contributes its disulfide to folding substrates is located on the enzyme surface, surrounded by hydrophobic patches thought to interact with unfolded or partly folded protein substrates. A hydrophobic groove adjacent to the C*XX*C motif binds to a redox-active periplasmic loop of the EcDsbB membrane protein during re-oxidation of EcDsbA (Inaba *et al.*, 2006).

A crystal structure of oxidized TcpG at 2.1 Å resolution has previously been reported (Hu *et al.*, 1997). The relatively flat surface of the enzyme around the active site suggested that the enzyme might not be suitable for the development of small-molecule inhibitors. The properties, structures and virulence functions of DsbA proteins from several bacterial organisms have been characterized, revealing a spectrum of redox characteristics and a variety of structural modifications that can be accommodated into the core fold (Shouldice *et al.*, 2011). However, the redox properties of TcpG have not been extensively characterized. Here, we present a comprehensive redox characterization of TcpG and report the high-resolution crystal structure of TcpG at 1.2 Å resolution. This is the highest resolution DsbA structure reported to date and the first DsbA crystal structure to include refined H atoms.

2. Materials and methods

2.1. Cloning, expression and purification

The *V. cholerae tcpg* gene (accession code P_32557) was amplified from the pTrc99A vector, a gift from R. K. Taylor (Dartmouth Medical College). Primers TcpG forward, 5′-TAC TTC CAA TCC AAT GCG GCT CAA TTT AAA GAA GG-3′, and TcpG reverse, 5′-TTA TCC ACT TCC AAT CCT ACT TCA GCG TCA GCA GG-3′, were used and were compatible with ligation-independent cloning. The PCR product was then inserted into a modified pET-21a vector encoding an N-terminal His_6 tag followed by a tobacco etch virus (TEV) protease-recognition site with an additional three amino acids encoded (Ser, Asn and Ala) before the gene sequence. The amplified gene contained two variants compared with the sequence in the UniProt sequence database (accession code P_32557): Arg134His and Val164Ala (numbering is for the mature protein after cleavage of the signal sequence). The Arg134His mutation was introduced during subcloning from pTrc99A into pET-21a. The Val164Ala mutation was present in the original pTrc99A vector and may represent an error in the database.

Competent *E. coli* BL21 (DE3) pLysS cells were transformed with the plasmid containing the *tcpg* gene and transformed cells were used for protein expression by auto-induction (Studier, 2005). Bacterial cultures were pelleted by centrifugation and the cell pellets were lysed in 50 ml lysis buffer (per litre of cell culture) consisting of 25 m*M* HEPES pH 7.5 (Biochemicals, Australia), 150 m*M* NaCl (Amresco, USA), 0.5% Triton X-100 (Chem-Supply, USA), EDTA-free protease-inhibitor cocktail (100 U; Roche, USA) and DNAse (100 U; Roche, Australia). The sample was sonicated and cell debris was removed by centrifugation. His_6-tagged TcpG was purified by metal-affinity chromatography using TALON resin (Clontech, Australia; 4 ml per litre of original cell culture). The resin was washed extensively with 25 m*M* HEPES, 150 m*M* NaCl, 20 m*M* imidazole (Amresco, USA) pH 7.5 and eluted with 25 m*M* HEPES, 150 m*M* NaCl, 500 m*M* imidazole pH 7.5. To remove the His_6 tag, 10 ml 1 mg ml^{-1} purified TcpG was incubated with 100 µl 1 mg ml^{-1} recombinant His-tagged TEV protease (Blommel & Fox, 2007) and dialyzed against 25 m*M* HEPES, 150 m*M* NaCl pH 7.0 at 277 K for 48 h. After dialysis, the TEV-treated protein sample was passed over TALON resin (4 ml) again to separate the His_6-tagged components from the cleaved TcpG. The protein was further purified by gel-filtration chromatography using a Superdex S75 16/60 column equilibrated with 10 m*M* HEPES, 150 m*M* NaCl pH 6.8 on an ÄKTA FPLC (GE Healthcare, USA).

Peak fractions containing TcpG were pooled, concentrated to 500 µ*M*, oxidized by the addition of copper(II) 1,10-phenanthroline (final concentration 1.7 m*M*) and incubated for 1 h at 277 K. The oxidizing agent was removed from the TcpG using a PD10 column (GE Healthcare, USA) with elution buffer 10 m*M* HEPES, 0.5 m*M* EDTA pH 8.3. The final purification step was anion-exchange chromatography using a Mono Q 5/50 GL column on an ÄKTA FPLC with a 0–500 m*M* NaCl gradient over 30 column volumes. Peak fractions from the eluant were pooled and concentrated to 7 mg ml^{-1} in 10 m*M* HEPES, 40 m*M* NaCl, 0.5 m*M* EDTA pH 6.8 using an Amicon centrifugal concentrator with a 10 kDa cutoff (Millipore). The protein concentration was measured at 280 nm using a NanoDrop ND-1000 (NanoDrop Technologies) and the protein purity was assessed by SDS–PAGE on a NuPAGE 4–12% bis-Tris gel (Invitrogen, Australia). The protein concentration was determined using a NanoDrop 2000 (Thermo Fisher Scientific, USA). An extinction coefficient of 10 555 M^{-1} cm^{-1} (calculated from the TcpG sequence using *ProtParam*; Gasteiger *et al.*, 2003) was used.

2.2. Crystallization and structure determination

Crystals of oxidized TcpG were grown by hanging-drop vapour diffusion by mixing 1 µl protein solution at 7 mg ml^{-1} and 1 µl crystallization solution consisting of 13% PEG 4000, 100 m*M* MES pH 6.4, similar to the conditions used for the 2.1 Å resolution room-temperature TcpG crystal structure (Hu *et al.*, 1997). The cryoprotectant contained an additional 4% PEG 400 and a cocktail of four ligands (5,5-dibromobarbituric acid, 2-hydroxy-4-methylquinoline, l-phenylalanine and 2-methoxyhydroquinone) at concentrations of 5 m*M* each in 10% DMSO. Crystals were soaked in the cryoprotectant for 2 h. None of the four ligands bound to TcpG, although two

DMSO molecules did bind. X-ray data were recorded on the microcrystallography beamline MX2 at the Australian Synchrotron using the *Blu-Ice* software (McPhillips *et al.*, 2002). Reflections were measured on an ADSC Quantum 315r Detector (ADSC, Poway, USA) at a wavelength of 0.9536 Å (13 000.5 eV). The crystal-to-detector distance was 150 mm. Oscillation images of 1° were collected for a total of 720 images using 2 s exposure per image. Diffraction data were indexed and integrated with *XDS* (Kabsch, 2010) and were scaled using *SCALA* (Evans, 2006). Phasing was performed by molecular replacement with *Phaser* (McCoy *et al.*, 2007) using the structure of PDB entry 1bed (Hu *et al.*, 1997). The final model was obtained after several rounds of model building in *Coot* (Emsley & Cowtan, 2004) and refinement in *PHENIX* (Afonine *et al.*, 2010). Structure validation was performed in *MolProbity* (Chen *et al.*, 2010).

Difference electron-density maps indicated evidence for H atoms (Supplementary Fig. S1[1]) and these were therefore included in refinement, initially using the riding model and finally using individual refinement (which lowered the $R_{\rm free}$ by a further 0.7%). The final model included the non-native residues Ser−2, Asn−1 and Ala0 at the N-terminus that originate from the engineered TEV cleavage site and residues 1–181 of the mature protein (without the signal sequence). Density for the side chains of Gln2, Lys4, Gln10, Lys13, Lys52, Gln162, Lys165 and Lys181 was relatively poor and these side chains were refined with occupancies of 0–0.5. The crystal structure showed signs of radiation damage, including partial decarboxylation of several acidic residues (Burmeister, 2000); affected side-chain atoms were refined with an occupancy of 0.8. Anisotropic refinement was used for all atoms (except for H atoms), including 284 water molecules (H atoms were not included on waters). In addition, two DMSO molecules and a sulfate were modelled in the structure and refined with an occupancy of 0.8. The sulfate was modelled because the density was not explained by modelling a water molecule and because the sulfate could be part of an MES molecule (MES was used in the crystallization buffer). However, no density was present for anything other than the modelled sulfate, so we cannot conclude definitively that sulfate or MES is bound. *MolProbity* (Chen *et al.*, 2010) was used to evaluate the crystal structure quality. Structural figures were prepared using *PyMOL* (DeLano, 2002). The electrostatic surface figure was generated by first using *PDB2PQR* (Dolinsky *et al.*, 2007) to determine the atomic charges for TcpG. The electrostatic potential calculation was performed using *APBS* (Baker *et al.*, 2001) with an ionic strength of 150 m*M*, a protein core dielectric constant of 2 and a solvent dielectric constant of 78. The surface electrostatic potential of TcpG was contoured from $-3kT$ per electron (red) to $+3kT$ per electron (blue) and the solvent-accessible surface option was selected for displaying the electrostatic surface charge within *PyMOL*. Coordinates and structure factors have been deposited in the PDB (entry 4dvc) and image files have been deposited in DIMER (http://xr-diffraction.imb.uq.edu.au/).

2.3. Preparation of EcDsbB and ubiquinone 1

The plasmid pQE-70 harbouring EcDsbB was a gift from Professor James Bardwell (University of Michigan). EcDsbB was expressed and purified as described previously (Bader *et al.*, 1998) with minor modifications to the buffer compositions. For cell lysis, a 1× PBS buffer solution (137 m*M* NaCl, 2.7 m*M* KCl, 100 m*M* Na_2HPO_4, 2 m*M* KH_2PO_4) with 50 U DNase and 50 U protease inhibitor per litre of culture was used and the cell pellets were homogenized using a 50 ml syringe. Membrane-protein solubilization was performed in 1× PBS buffer and 1% dodecyl-β-D-maltoside (β-DDM; Affimetrix, USA).

To prepare ubiquinone 1 (UQ1), a 0.85 m*M* solution of 2,3,4-trimethoxy-6-methyl-5-prenylphenol (225 mg in 2 ml 100% ethanol) was diluted with 10 ml water and an excess of $FeCl_3$ (8.5 m*M*) was added. The mixture was stirred at room temperature for 2 h and then extracted with three 10 ml portions of ethyl acetate. The organic extracts were pooled and washed with three portions of brine (5 ml of saturated NaCl/water solution) to give UQ1 as a pure product (220 mg, >95%). Physicochemical data for UQ1 were in agreement with the literature (Liang & Fener, 2004).

2.4. Redox-potential measurements

Oxidized TcpG (2 µ*M*) was incubated in fully degassed buffer consisting of 100 m*M* sodium phosphate, 1 m*M* EDTA pH 7.0 containing 1 m*M* oxidized glutathione (GSSG; Sigma–Aldrich, USA) and a range of reduced glutathione (GSH) concentrations (0.1 µ*M*–2 m*M*) for 24 h at room temperature. After incubation, the reactions were stopped with 10% trichloroacetic acid (TCA) and the precipitated protein pellets were collected by centrifugation at 14 000 rev min^{-1} for 10 min at 277 K. The pellets were washed with 100% ice-cold acetone and dissolved in a buffer consisting of 50 m*M* Tris–HCl pH 7.0, 1% SDS, 4 m*M* 4-acetamide-4′-maleimidyl-stilbene-2,2′-disulfonate (AMS) to label the free thiols. Separation of the reduced and oxidized forms was performed on a NuPAGE 12% bis-Tris gel (1.0 mm thick, 12-well; Invitrogen, Australia). The gel was stained with Coomassie Brilliant Blue and scanned: the relative intensity of the reduced and oxidized forms was analyzed using *ImageJ* v.1.42q (Abramoff *et al.*, 2004). The fraction of the reduced protein was plotted against the ratio $[GSH]^2/[GSSG]$, and the equilibrium constant $K_{\rm eq}$ was calculated using the equation

$$R = \frac{[GSH]^2}{[GSSG]} \Big/ \left(K_{\rm eq} + \frac{[GSH]^2}{[GSSG]} \right), \qquad (1)$$

where R is the fraction of reduced protein at equilibrium. The standard redox potential was calculated using the Nernst equation,

$$E^{0'} = E^{0'}_{\rm GSH/GSSG} - \frac{RT}{nF} \ln K_{\rm eq}, \qquad (2)$$

[1] Supplementary material has been deposited in the IUCr electronic archive (Reference: BE5204). Services for accessing this material are described at the back of the journal.

where $E^{0\prime}_{GSH/GSSG}$ is the standard potential of −240 mV (Gilbert, 1995), R is the universal gas constant 8.314 J K^{-1} mol^{-1}, T is the absolute temperature in kelvin, n is the number of electrons transferred, F is the Faraday constant 9.648 × 10^4 C mol^{-1} and K_{eq} is the equilibrium constant.

2.5. Melting-temperature measurements

Thermal unfolding was performed by measuring the CD spectrum on a J-810 spectropolarimeter (Jasco, USA). Unfolding of reduced or oxidized TcpG was induced by increasing the temperature from 298 to 368 K with a heating rate of 1 K min^{-1}. For both proteins, the conditions used were 10 µ*M* protein in 100 m*M* sodium phosphate and 1 m*M* EDTA pH 7.0. The redox state of the oxidized protein was verified by Ellman's assay. Thermal unfolding measurements of reduced TcpG were performed in the presence of 0.75 m*M* DTT. Unfolding was monitored by circular-dichroism measurements and was analysed using *Spectra Manager* (Jasco, USA). Three replicates were measured for each of the reduced and oxidized enzymes. Thermal unfolding was calculated using a two-state model (Pace *et al.*, 1998),

$$y = \frac{(y_f + m_f T) + (y_u + m_u T) \times \exp\left[\dfrac{-\Delta H_m}{RT} \times \dfrac{T - T_m}{PT_m}\right]}{1 - \exp\left[\dfrac{-\Delta H_m}{RT} \times \dfrac{T - T_m}{PT_m}\right]}, \quad (3)$$

where y is the observed far-UV circular-dichroism signal at 221.5 nm for oxidized protein and at 219.5 nm for reduced protein, y_f is the intercept for the folded protein, m_f is the slope of the pre-translational baseline, y_u is the intercept for the unfolded protein, m_u is the slope of the post-translational baseline, T is the temperature, T_m is the midpoint of the thermal unfolding curve and ΔH_m is the enthalpy change for unfolding at T_m.

2.6. Insulin-reduction assay

The protein disulfide reductase activity of TcpG was measured *in vitro* using the insulin-reduction assay in the presence of DTT (Holmgren, 1979). 10 µ*M* EcDsbA (as a positive control) or 10 µ*M* TcpG were mixed with buffer consisting of 100 m*M* sodium phosphate, 2 m*M* EDTA, 0.33 m*M* DTT. 0.131 m*M* insulin was added immediately before measurements were made. Insulin comprises an A and a B chain connected by two disulfide bonds. Reduction of the disulfide bonds leads to precipitation of the insoluble B chain, and this can be followed as an increase in optical density at 650 nm. The solutions were monitored at 30 s intervals over a period of 80 min on a Cary 50 UV–visible spectrophotometer (Varian).

2.7. Motility assay with complemented *dsbA*$^-$ mutants in *E. coli*

E. coli strains JCB570 (wild type) and JCB571 (*dsbA*$^-$ mutant) were kindly provided by Professor James Bardwell (University of Michigan). JCB571 was transformed chemically (Chung & Miller, 1988) with the gene encoding *tcpg* (without the Arg134His mutation) cloned into a pTrc vector. Motility assays were performed essentially as described previously (Macnab, 1986) in M63 minimal medium containing agar (0.3%) supplemented with each essential amino acid except for cysteine and cystine (40 µg ml^{-1}). All strains (JCB570, JCB571 and JCB571*pvcdsbA*) were grown as streak cultures overnight on LB–agar plates at 310 K. Motility assays were performed in triplicate using single colonies from the overnight plate, which were inoculated by stabbing the centre of the M63 soft agar plate. Plates were incubated for 7–12 h and the diameter of the zone of swarming was measured manually.

2.8. Peptide-oxidation assay

The peptide CQQGFDGTQNSCK, with a 1,4,7,10-tetraazacyclododecane-1,4,7,10-tetraacetic acid (DOTA) group amide-coupled to the N-terminus and a methylcoumarin amide-coupled to the ε-amino group of the C-terminal lysine, was purchased from AnaSpec. The lyophilized peptide was resuspended in 100 m*M* MES pH 6 at a concentration of ∼1 m*M*. Europium trifluoromethanesulfonate was dissolved to a concentration of 100 m*M* in 100 m*M* MES pH 6. The europium was added to the peptide sample to a molar ratio of 3:1 and then incubated for 5 min at room temperature. Tris-(2-carboxyethyl)phosphine hydrochloride (TCEP) was added to a 5:1 molar ratio compared with peptide and then incubated for 5 h at 310 K.

Reverse-phase HPLC was run on a Waters preparative liquid-chromatography system. A 250 × 21.20 mm Phenomenex Luna C8(2) column with 8–10 µm particle size and 100 Å pore diameter was used at a flow rate of 20 ml min^{-1}. Peptide elution was monitored by UV absorbance at 254 nm. The column was pre-equilibrated in 0.1% TFA. The reduced peptide sample was brought to 0.1% TFA immediately before loading and injection. The peptide sample was injected onto the column and then washed with five column volumes of 0.1% TFA. The peptide was eluted with a 0–80% acetonitrile gradient (in the presence of 0.1% TFA) over 45 min (250 × 21.20 mm column). The purified peptide was immediately flash-cooled in liquid nitrogen and freeze-dried. The lyophilized peptide was stored at 253 K.

TcpG (Arg134His/Val164Ala) was prepared as described above, native TcpG (Val164Ala) was expressed and purified as described previously (Bader *et al.*, 1998) and DsbB membrane suspensions were expressed and purified as described in Horne *et al.* (2007). EcDsbA was expressed and purified as described in Paxman *et al.* (2009).

Assays were run on a Perkin Elmer Envision plate reader/fluorimeter. A Photometric 340 narrow excitation filter and a Cy5 620 emission filter were used, with a 100 ms delay before reading and a 400 ms reading time. 384-well Perkin Elmer White OptiPlate-384 plates were used. Prior to commencing the assay, 25 µl solutions consisting of 780 n*M* DsbB (in membrane suspension), 20–40 n*M* TcpG in 50 m*M* MES, 50 m*M* NaCl, 2 m*M* EDTA pH 5.5 were added to the plate

Table 1
X-ray data-collection and refinement statistics for TcpG.

Values in parentheses are for the highest resolution shell. Except for the *MolProbity* analysis, statistics for 1bed are those reported previously (Hu *et al.*, 1997) and those for the *PDB_REDO* re-refined 1bed-final were taken from the *PDB_REDO* website (Joosten *et al.*, 2012).

	1bed	1bed-final	4dvc
Data collection			
Wavelength (Å)	1.5418		0.95369
Resolution range (Å)	40–2.0 (2.07–2.00)		64.3–1.2 (1.26–1.20)
Space group	$C222_1$		$C222_1$
Unit-cell parameters (Å, °)	a = 64.0, b = 91.5, c = 64.8, $\alpha = \beta = \gamma$ = 90		a = 62.65, b = 89.52, c = 64.26, $\alpha = \beta = \gamma$ = 90
No. of molecules in asymmetric unit	1		1
Observed reflections	60945		793759 (104951)
Unique reflections	12974 (681)		56674 (8105)
R_{merge}	0.062 (0.341)		0.103 (1.11)
$R_{p.i.m.}$	—		0.029 (0.319)
Completeness (%)	98.2 (91.7)		99.8 (98.7)
$\langle I/\sigma(I)\rangle$	23.5 (3.4)		18.0 (3.1)
Multiplicity	5.7 (2.9)		14.0 (12.9)
Refinement			
Resolution (Å)	20–2.1 (2.15–2.10)	52–2.0 (2.05–2.00)	32.1–1.2 (1.23–1.20)
R factor	0.205 (0.277)	0.175 (0.253)	0.119 (0.194)
R_{free}†	0.241 (0.368)	0.201 (0.295)	0.139 (0.194)
No. of atoms			
Protein [including H]	1385	1454	1489 [2976]
Waters	52	252	284
DMSO	—	—	2 × 8
Sulfate	—	—	1 × 5
B factors (Å^2)			
Wilson	31		10.0
Protein/water/DMSO/sulfate	38.2 (all atoms)	17.1	15.0/29.3/32.4/25.0
R.m.s.d. from ideal geometry			
Bonds (Å)	0.007	0.011	0.007
Angles (°)	1.2	1.2	1.2
MolProbity analysis			
Ramachandran favoured/outliers (%)	96.6/0.6	97.8/0.0	98.9/0.0
Residues with bad angles (%)	1.66	0.55	0.0
Poor rotamers (%)	3.6	3.2	0.0
Clashscore [percentile]	10.95 [78th]	6.29 [95th]	2.48 [97th]
MolProbity score [percentile]	2.19 [58th]	1.78 [87th]	1.03 [98th]

† R_{free} was calculated from 10% (931 reflections) and 3.5% (2000 reflections) of the diffraction data for 1bed and 4dvc, respectively. These were selected randomly and excluded from refinement.

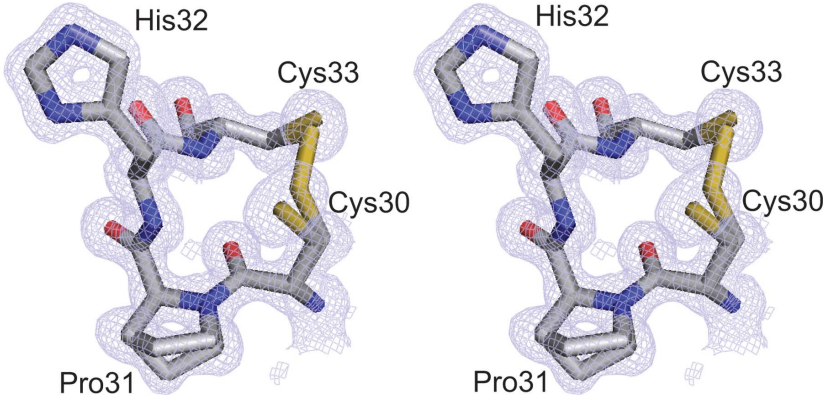

Figure 1
Active site of TcpG. The modelled Cys30, Pro31, His32 and Cys33 residues of the C*XX*C active-site motif are shown in stick representation (H atoms were removed for clarity). The $2F_o - F_c$ map was created using *FFT* in the *CCP*4 suite (Winn *et al.*, 2011) and is contoured at 1.0σ. Although the protein was crystallized in the oxidized form, the structure was modelled with a partial disulfide bond (*i.e.* a mixture of oxidized and reduced cysteines for Cys30 and Cys33). Reduction of disulfide bonds is often observed after X-ray exposure of crystals (Burmeister, 2000; Shimizu *et al.*, 2007), especially for redox-active cysteines such as those in thioredoxin and DSB proteins (Roberts *et al.*, 2005; Rozhkova *et al.*, 2004).

wells. The assay was initiated by the addition of 25 µl 16 µ*M* peptide (in 50 m*M* MES, 50 m*M* NaCl, 2 m*M* EDTA pH 5.5) to each well.

2.9. Ubiquinone-reduction assay

The enzyme EcDsbB oxidizes EcDsbA in a reaction that requires UQ1. During the reaction, UQ1 is reduced by EcDsbB and this can be monitored as a decrease in the absorbance at 275 nm. To determine whether TcpG was a substrate of EcDsbB, we followed the reduction of UQ1 using a Varian Cary 50 UV–visible spectrophotometer. For the assay, 30 µ*M* reduced TcpG was mixed with 30 µ*M* UQ1 and 40 n*M* purified EcDsbB in 0.1% β-DDM, 50 m*M* Tris, 100 m*M* NaCl pH 8.0 at 303 K. Reduced EcDsbA was used in place of TcpG as a positive control reaction. As negative controls, TcpG was either mixed with EcDsbB in the absence of UQ1 or mixed with UQ1 in the absence of EcDsbB and the reactions were started immediately after mixing. The initial rate of reaction was analyzed in *GraphPad Prism* v.5.0d (GraphPad Software, La Jolla California, USA) using the one-phase exponential decay equation, giving a calculated rate constant K with standard error. Three replicates were measured using the same batches of TcpG, EcDsbA and EcDsbB.

3. Results

3.1. High-resolution structure of TcpG

We measured high-resolution data from a cryocooled crystal of TcpG that had been cryoprotected in a solution containing DMSO. The crystal structure was solved by molecular replacement using the previously determined room-temperature crystal structure of TcpG at 2.1 Å resolution (PDB entry 1bed; Hu *et al.*, 1997; Table 1). The new TcpG crystal structure (PDB entry 4dvc) was refined to a resolution of 1.2 Å and shows the typical DsbA topology of a thioredoxin fold comprising a C*XX*C active-site motif (Fig. 1) with an inserted helical domain.

Superimposition of the cryocooled high-resolution structure and the room-temperature structure 1bed solved at 2.1 Å resolution gives a root-mean-square deviation (r.m.s.d.) of 0.64 Å for 172 C^{α} atoms. Although the overall folds are identical, there are localized differences in the structure. For example, the short loop comprising residues 161–167 that connects strand $\beta5$ to the C-terminal helix $\alpha7$ adopts different conformations in the two structures (Fig. 2). The equivalent loop in EcDsbA is six residues longer than in TcpG; it is also flexible and forms one edge of a hydrophobic groove that binds the periplasmic loop of EcDsbB. The $\beta5$–$\alpha7$ loop is relatively disordered in the 1bed structure, with most of the side chains not included in the model. The recently re-refined 1bed structure (1bed_final from the *PDB_REDO* team; Joosten *et al.*, 2012) is a much improved model (Table 1), but the loop remains poorly ordered, especially residues Gln162, Ser164, Val164 and Lys165. The conformation of the loop is similar in 1bed and 1bed_final. By comparison, the equivalent loop in the high-resolution structure is relatively well ordered, with excellent density for the main-chain atoms and almost all side chains modelled. The main-chain conformation of the loop differs between the 4dvc and 1bed TcpG structures, with an r.m.s.d. of 0.65 Å for the C^{α} atoms of residues 161–167. These results suggest that the C-terminal $\beta5$–$\alpha7$ loop of TcpG is more flexible than the rest of the structure and this is likely to be important for its role in binding the periplasmic loop of DsbB. This finding supports the conclusions of Horne and coworkers that this loop is mobile in solution (Horne *et al.*, 2007) as shown by relatively few NOE constraints and because proteolytic cleavage was found to occur first at Lys165 in the $\beta5$–$\alpha7$ loop. Furthermore, NMR dynamic studies of TcpG (Horne *et al.*, 2007) identified a domain-hinge motion unique to reduced TcpG. This hinging motion was thought to favour opening of the $\beta5$–$\alpha7$ loop to facilitate binding of the DsbB periplasmic loop in the hydrophobic groove of the reduced protein (Horne *et al.*, 2007).

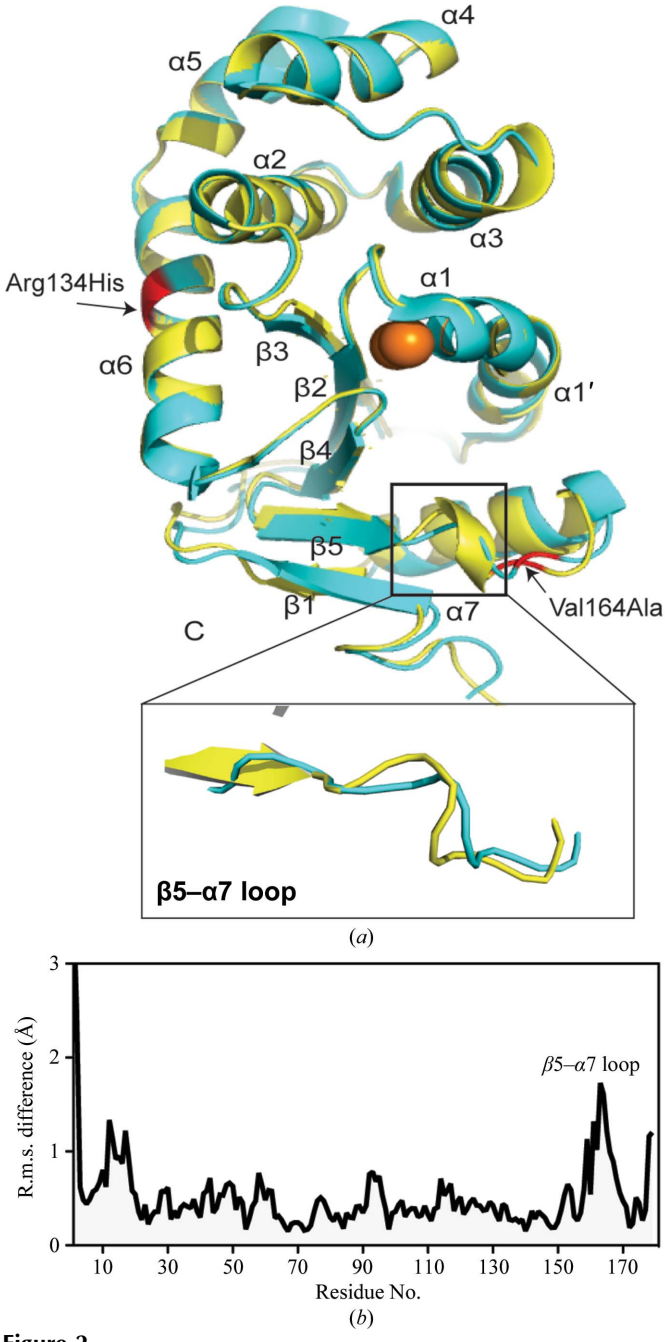

Figure 2
Comparison of the 1.2 and 2.1 Å resolution TcpG structures. (*a*) The two structures were superimposed, with the 1.2 Å resolution structure shown in yellow and the 2.1 Å resolution structure 1bed shown in cyan. The sulfurs of the active-site cysteines are shown as orange spheres. The boxed region highlights the conformational variation between the two crystal structures in the region of the $\beta5$–$\alpha7$ loop. The positions of the two mutated residues (Arg134His and Val164Ala) in the polypeptide chain are highlighted in red. (*b*) Plot of C^{α}-atom r.m.s.d. for the comparison of the 1.2 Å resolution TcpG structure with the 2.1 Å resolution crystal structure 1bed (calculated using the *SUPERPOSE* program in the *CCP*4 suite; Winn *et al.*, 2011). The plot was prepared using *GraphPad Prism* v.5.0d (GraphPad Software, La Jolla, California, USA). The plot highlights that the largest differences between the two structures are at the N- and C-termini and in the $\beta5$–$\alpha7$ loop.

The N-terminal residues also exhibit local differences between the high-resolution TcpG structure and 1bed, as can be seen in the distribution of r.m.s.d. values for main-chain atoms (Fig. 2*b*; r.m.s.d. of 1.0 Å for the 19 N-terminal C^{α} atoms). Similarly, the r.m.s.d. is 1.4 Å for the 19 N-terminal C^{α} atoms of the high-resolution TcpG structure in comparison with the NMR structure of reduced TcpG; PDB entry 2ijy; Horne *et al.*, 2007) and 2.1–2.5 Å for comparison with EcDsbA (PDB entry 1fvk, chains *A* and *B*; Guddat *et al.*, 1997). Clearly, the N-terminus of TcpG, like that of many proteins, is relatively flexible, even though it adopts the same overall topology and secondary structure in each of these structures.

3.2. Small-molecule binding sites

DMSO was included in the cryoprotectant solution used for TcpG crystal soaking prior to diffraction data collection. The resulting electron-density map revealed two regions that bind DMSO (which we modelled as DMSO1 and DMSO2) and a binding site at the N-terminus that was modelled as a sulfate.

DMSO1 and DMSO2 bind in two pockets, as shown in Fig. 3(*a*). DMSO1 binds in a cavity between the thioredoxin and helical domains of TcpG on the opposite face of the

molecule to the active-site surface. The DMSO1 pocket is formed by the side chains of Glu37, Lys55, Tyr73, Glu82, Asp83 (Fig. 3*b*) and Val86 (not shown). DMSO2 binding is not as well defined and the density suggests more than one binding mode. Residues forming the DMSO2 site are contributed by the N- and C-termini of TcpG: Ser19, Pro20, Asn154 and Lys181 (Fig. 3*c*). Additional density was observed at a crystal contact point including interactions with the N-terminal engineered residues Ser−2 and Asn−1. This density was modelled as a sulfate (Fig. 3*a*).

3.3. TcpG is more active than EcDsbA in the insulin-reduction assay

We tested TcpG for its ability to catalyze the reduction of insulin in the classic redox-activity assay. Insulin comprises two chains, A and B, linked by two disulfide bonds. The B chain is insoluble and reduction of the disulfide bonds leads to B-chain precipitation, which can be monitored as an increase in absorbance at 650 nm. Under the standard assay conditions, the disulfide isomerase *E. coli* DsbC (EcDsbC) catalyzes insulin reduction by DTT. This results in precipitation of the B chain and a consequent increase in the OD_{650} which is measurable after 7 min (Shevchik *et al.*, 1994). EcDsbA-mediated catalysis was slower than that mediated by EcDsbC, with the increase in OD_{650} being measurable after 15 min (Wunderlich *et al.*, 1993). TcpG-mediated DTT reduction of insulin occurs relatively quickly, being measurable after 7 min (Fig. 4*a*). Therefore, in this assay under these conditions the activity of TcpG is more similar to that of the bacterial disulfide isomerase EcDsbC than to that of the bacterial dithiol oxidant EcDsbA.

3.4. TcpG is as oxidizing as EcDsbA

When it was first characterized, EcDsbA was described as the most oxidizing thioredoxin-like protein, with a redox potential of −122 mV (Huber-Wunderlich & Glockshuber, 1998). By comparison, the disulfide-reducing protein *E. coli* thioredoxin has a redox potential of −270 mV (Aslund *et al.*, 1997). Compared with EcDsbA, the redox-potential values of other DsbA proteins vary from more reducing (*e.g.* α-DsbA1 from *Wolbachia pipientis*, $E^{0\prime} = -163$ mV; Kurz *et al.*, 2009) to more oxidizing (*e.g.* NmDsbA3 from *Neisseria meningitidis*, $E^{0\prime} = -89$ mV; Vivian *et al.*, 2009). We determined the standard redox potential of TcpG relative to the redox potential of GSH/GSSG (−240 mV). The equilibrium constants were determined from the calculated fraction of reduced TcpG at different concentrations of $[GSH]^2/[GSSG]$ (Fig. 4*b*). From these data, the K_{eq} for TcpG was $7.7 \pm 0.03 \times 10^{-5}$ *M* and the corresponding redox potential was −116 mV at pH 7.0. Thus, in the spectrum of redox potentials for thioredoxin-fold proteins TcpG is relatively oxidizing, with a redox-potential value similar to that of EcDsbA.

The active-site cysteine of EcDsbA has an unusually low pK_a of ∼3.5 (Nelson & Creighton, 1994), which is thought to be important for redox activity since the thiolate form of the reduced side chain is favoured at physiological and acidic pH. We made several attempts to measure the pK_a of the active-site cysteine of TcpG using a range of different buffers. However, we found that reduced TcpG precipitates at pH values of −5 and below and we were thus unable to measure the pK_a of TcpG Cys30.

3.5. Reduced TcpG is more stable than oxidized TcpG

TcpG contains no Trp residues and does not exhibit intrinsic fluorescence, unlike other DsbA proteins such as EcDsbA. Therefore, its thermal stability cannot be assessed using changes in

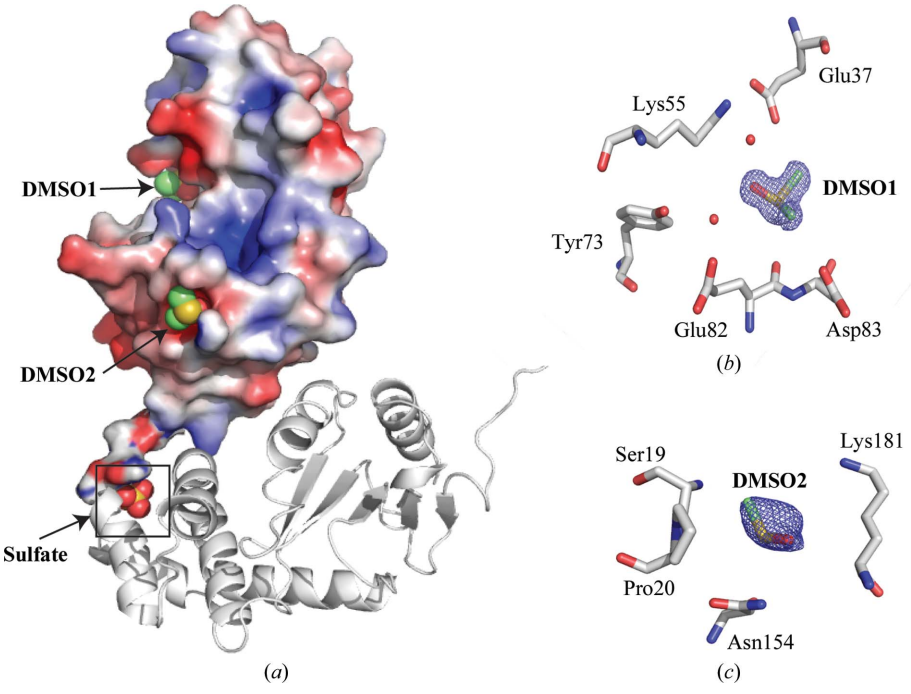

Figure 3
Electrostatic surface of TcpG showing small-molecule binding sites. (*a*) The electrostatic potential is plotted on the molecular surface of TcpG, with charge levels from $-3kT$/e (red) to $+3kT$/e (blue). *PDB2PQR* was used to assign atomic charges and radii based on the PARSE force field and the electrostatic potential calculation was performed using the *APBS* software (Dolinsky *et al.*, 2004). The two DMSO molecules and one sulfate molecule that were modelled into the electron density are shown as space-filling models and their positions are identified with labels and arrows. A box also highlights the bound sulfate located at a crystal contact point: a symmetry-related molecule of TcpG (white) is shown forming part of the sulfate-binding site. (*b*) DMSO1 is shown with associated $2F_o - F_c$ electron density contoured at 1.0σ. The binding site is located between the helical and thioredoxin domains of TcpG. Two waters are shown as red spheres: these mediate hydrogen bonds to Lys55 and Tyr73. For clarity, Val86, which forms part of this site, is not shown. (*c*) DMSO2 is shown with associated $2F_o - F_c$ electron density contoured at 1.0σ. Nearby residues are also shown.

intrinsic fluorescence. We investigated the relative stability of the two redox forms of TcpG using circular dichroism (CD) by observing changes in CD during thermal unfolding of reduced and oxidized forms of the enzyme over the temperature range 298–368 K at pH 7.0 (Fig. 5*a*). The thermal transition values calculated from these data showed that the melting temperature of reduced TcpG is higher than that of oxidized TcpG by 11 K (T_m oxidized = 346 ± 0.1 K, T_m reduced = 357 ± 0.3 K). These results are in excellent agreement with previous data for TcpG measured by differential scanning calorimetry (T_m oxidized = 346 K, T_m reduced = 357 K; Horne *et al.*, 2007). The reduced form of TcpG is therefore more stable than oxidized TcpG, indicating that disulfide formation at the active site destabilizes TcpG. This is also the case for EcDsbA (Huber-Wunderlich & Glockshuber, 1998), although the difference in melting temperature is larger for TcpG than for

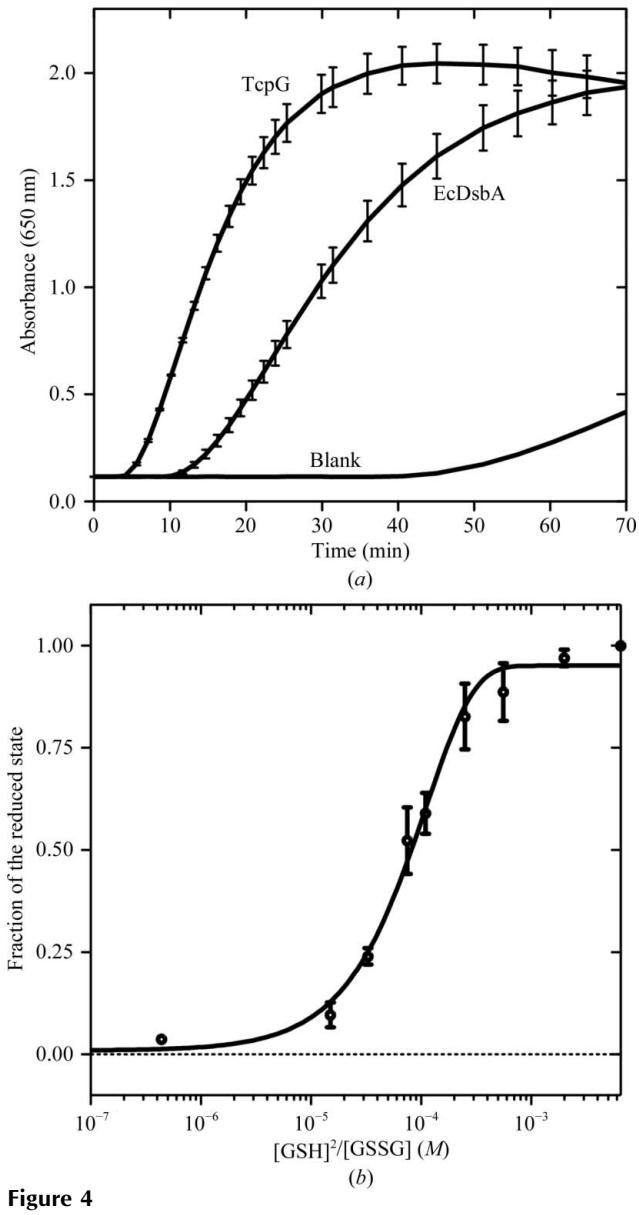

Figure 4
Characterization of the redox properties of TcpG. (*a*) The disulfide-reductase activity of TcpG was assessed using the insulin-reduction assay. 10 µ*M* TcpG or 10 µ*M* EcDsbA was used to catalyze the reaction in the presence of 131 µ*M* insulin in 100 m*M* sodium phosphate buffer pH 7.0, 2 m*M* EDTA, 330 µ*M* DTT. The curve labelled 'blank' contained all components except DsbA/TcpG. The data are representative of three independent experiments. (*b*) Nonlinear fit to the fraction of reduced TcpG at different ratios of reduced:oxidized glutathione. This fit was used to obtain the equilibrium constant K_{eq} and the redox potential (calculated relative to the GSH/GSSG standard potential of −240 mV; Gilbert, 1995). The curve was fitted to the averaged data from three replicate experiments (the mean and standard deviation of each point is shown).

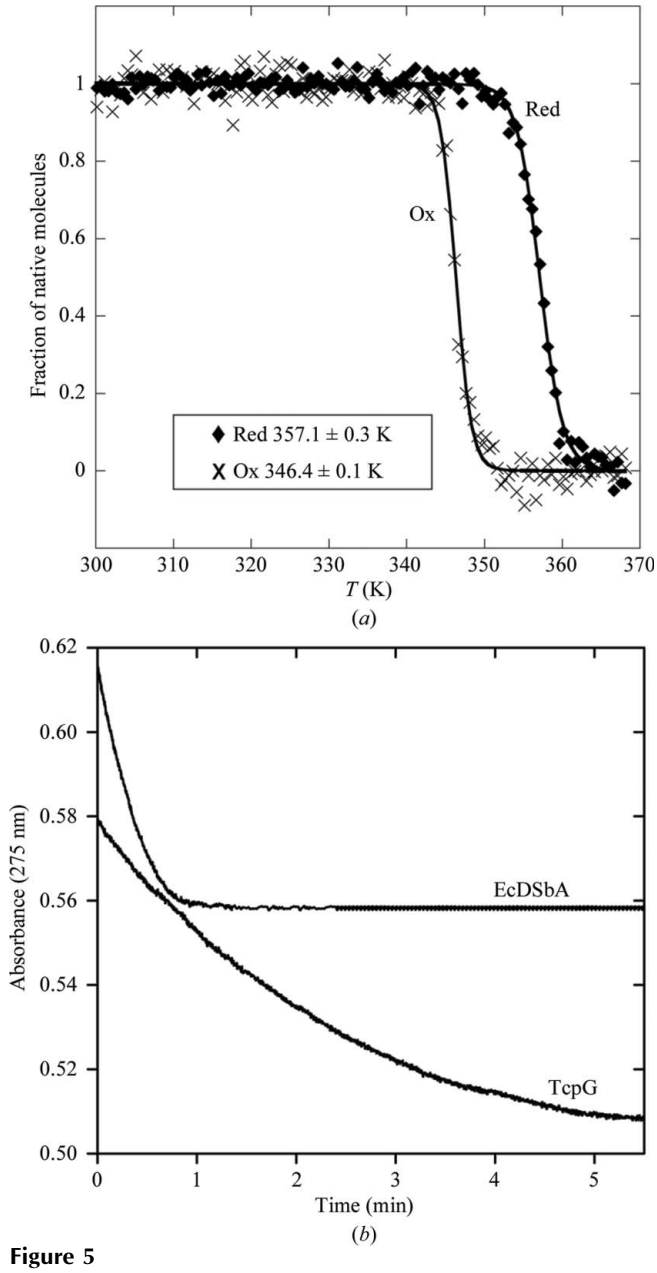

Figure 5
Relative stability of reduced and oxidized TcpG and the interaction of reduced TcpG with EcDsbB. (*a*) This plot shows the thermal unfolding of TcpG measured in 100 m*M* sodium phosphate and 1 m*M* EDTA at pH 7.0 with 10 µ*M* oxidized (squares) or reduced (diamonds) TcpG. (*b*) Ubiquinone reduction of EcDsbB–UQ1 by TcpG. 30 µ*M* reduced TcpG or 30 µ*M* EcDsbA as a positive control was mixed with EcDsbB and the reaction was started by adding UQ1. UQ1 reduction was monitored at 275 nm. (The difference in starting absorbance arises from the differing intrinsic fluroescence of EcDsbA and TcpG.) The data presented in (*a*) and (*b*) are representative of three experiments.

EcDsbA (ΔT_m TcpG = 11 K; ΔT_m EcDsbA = 8 K; Huber-Wunderlich & Glockshuber, 1998). These results also highlight that either CD or differential scanning calorimetry can be used to accurately measure T_m for DsbA proteins which lack a tryptophan residue.

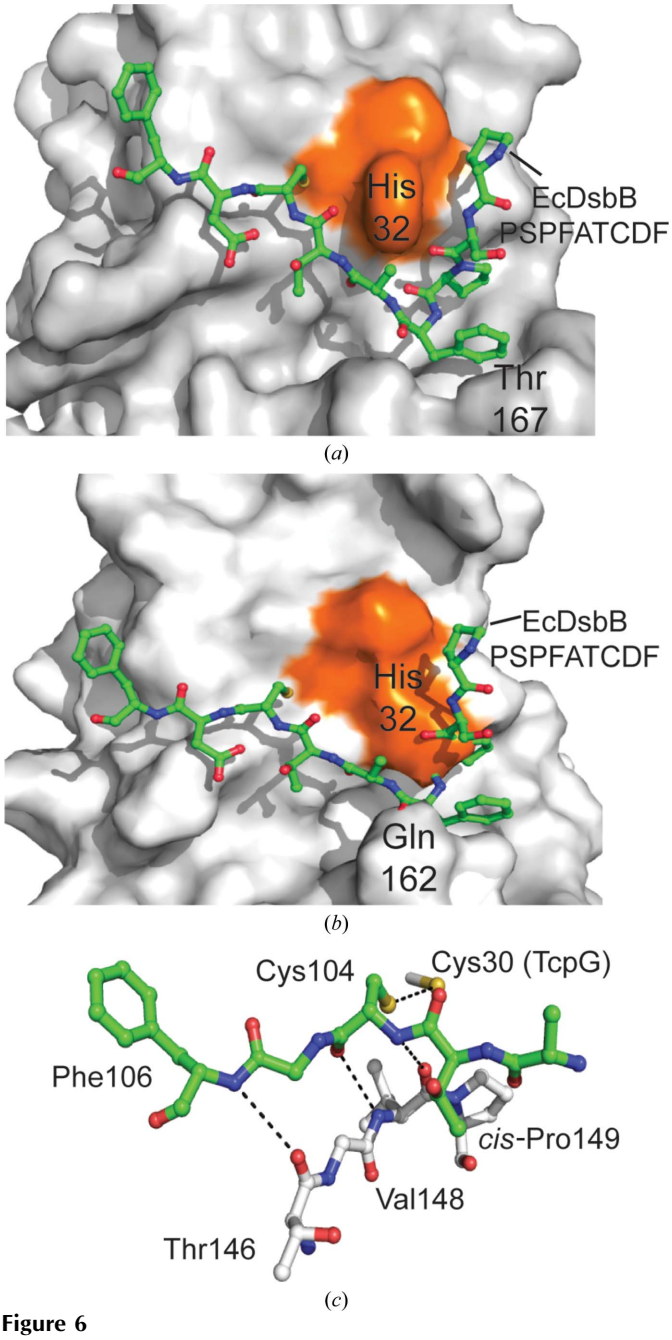

Figure 6
Model of the interaction of TcpG with EcDsbB. (*a*) Surface representation of EcDsbA (white) and its interaction with the periplasmic loop of EcDsbB 99-PSPFATCDF-106 (green stick format; Pro99 is on the far right-hand side in this orientation). The active site of EcDsbA is coloured orange and the His32 side chain is labelled. Thr167 from the flexible $\beta5$–$\alpha7$ loop is also labelled. This figure is derived from the crystal structure of the *E. coli* DsbA–DsbB complex (Inaba *et al.*, 2006). (*b*) TcpG was superimposed onto the structure of EcDsbA from the DsbA–DsbB complex and the overlay of the DsbB periplasmic loop is shown using the same colour scheme as above. Gln162 from the flexible $\beta5$–$\alpha7$ loop is labelled. (*c*) The interactions observed between *E. coli* DsbA and DsbB could also occur for TcpG. TcpG residues are shown in white, EcDsbB residues in green and potential hydrogen-bond interactions are shown as dashed lines. The intermolecular disulfide between Cys104 of DsbB and Cys30 of TcpG is also indicated by a dashed line.

3.6. TcpG interacts with EcDsbB

UQ1 acts as an electron acceptor in the EcDsbB–EcDsbA reaction: EcDsbB oxidizes the active-site thiols of reduced EcDsbA and passes the electrons to bound UQ1 (Bader *et al.*, 2000; Inaba & Ito, 2002). UQ1 reduction can be measured as a change in absorbance at 275 nm. Thus, when reduced EcDsbA is mixed with EcDsbB and UQ1 the absorbance at 275 nm decreases rapidly, indicating a redox interaction between the components. We found that when TcpG is used in place of EcDsbA, UQ1 is steadily reduced and the reaction is complete in 5 min (Fig. 5*b*). These findings show that TcpG can be oxidized by the homologous EcDsbB/UQ1 system, although the initial rate of UQ1 reduction by TcpG–EcDsbB is slower than that by EcDsbA–EcDsbB (the rate constants are 0.4 $\pm$ 0.01 and 3.2 $\pm$ 0.01 min^{-1}, respectively).

The amino-acid sequence (98-PSPFATCDF-105) of the EcDsbB periplasmic loop that is observed to interact with EcDsbA in the crystal structure of the complex (Inaba *et al.*, 2006) is highly conserved in the *V. cholerae* DsbB homologue (Supplementary Fig. S2). This conservation suggests that the VcDsbB loop residues might interact with TcpG in the same way that the equivalent EcDsbB residues interact with EcDsbA. The EcDsbA–EcDsbB crystal structure (PDB entry 2hi7; Inaba *et al.*, 2006) reveals that the EcDsbB periplasmic loop adopts a relatively extended conformation that loops around the active-site residue His32 of EcDsbA with a turn centred on residue Phe101 of EcDsbB. This Phe101 residue makes extensive interactions with the EcDsbA hydrophobic groove (Fig. 6*a*). A disulfide is formed between Cys104 of EcDsbB and Cys30 of EcDsbA (S—S distance of 2 Å) and backbone hydrogen-bond interactions appear to be formed with residues in the *cis*-proline loop of EcDsbA (EcDsbA Val150 O to EcDsbB Cys104 N, 3.5 Å; EcDsbA Val150 N to EcDsbB Cys104 O, 3.6 Å; EcDsbA Arg148 O to EcDsbB Phe106 N, 3.3 Å).

To examine whether similar interactions could be formed with TcpG, we superimposed the high-resolution crystal structure of TcpG onto the structure of EcDsbA from the EcDsbA–EcDsbB complex. Fig. 6(*b*) shows that the EcDsbB binding mode for the PSPFATCDF residues could be adopted but would require rotation of the side chain of TcpG active-site residue His32 (which otherwise blocks the EcDsbB loop) as well as movement of the $\beta5$–$\alpha7$ loop (Gln162 of the TcpG $\beta5$–$\alpha7$ loop blocks the EcDsbB loop). Movement of the $\beta5$–$\alpha7$ loop is possible since the loop appears to be flexible, as indicated above. Moreover, the superimposed model of the DsbB periplasmic loop supports the similar formation of an intermolecular disulfide (S—S distance of 3 Å) and potential hydrogen-bond interactions between DsbB and the *cis*-proline loop of TcpG (Fig. 6*c*; TcpG Val148 O to EcDsbB Cys104 N, 2.7 Å; TcpG Val148 N to EcDsbB Cys104 O, 3.1 Å; TcpG Thr146 O to EcDsbB Phe106 N, 3.2 Å).

3.7. TcpG oxidizes cysteines in proteins and peptides

The ability of TcpG to rapidly reduce insulin disulfides raised the question of whether TcpG is primarily an oxidant, a reductant or an isomerase. We tested this in two ways. Firstly, we determined whether TcpG could complement EcDsbA in a motility assay. EcDsbA is required for the oxidative folding of FlgI, a protein essential for producing functional flagella in *E. coli* (Dailey & Berg, 1993). In the absence of EcDsbA, *E. coli* are nonmotile on soft agar (Dailey & Berg, 1993). We tested whether native TcpG (Val164Ala) was able to complement EcDsbA in this assay and found that TcpG did indeed restore the motility of *E. coli* in this assay (Fig. 7). This indicates that TcpG, like EcDsbA, is able to act as an oxidant to form disulfides in FlgI.

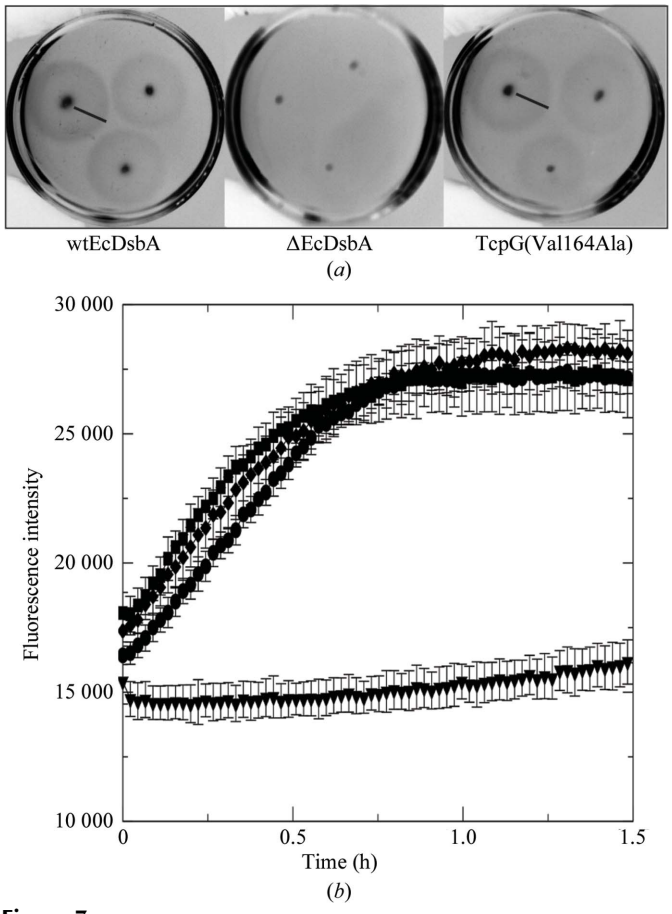

Figure 7
TcpG catalyzes disulfide formation *in vivo* and *in vitro*. (*a*) JCB570 *E. coli* wild-type cells are able to swarm on soft agar because they produce functional flagella (swarming is evident as a halo around the original stab point; left panel). In the absence of EcDsbA *E. coli* do not produce functional flagella because FlgI, an essential component of flagellar assembly, requires a disulfide bond (no swarming is evident; middle panel). TcpG (Val164Ala) is able to complement this nonmotile phenotype (right panel) as shown by the halo around the originial stab point with a diameter similar to that in the left panel (right panel). (*b*) Fluorescence curves representative of peptide oxidation are shown in the presence of 80 n*M* TcpG (Val164Ala) (squares), 80 n*M* TcpG (Arg134His/Val164Ala) (diamonds), 80 n*M* EcDsbA as a positive control (circles) and no TcpG/DsbA as a negative control (triangles). All three enzymes display a similar rate of peptide oxidation under these conditions, which is significantly faster than the negative control.

We also investigated the ability of TcpG to catalyze disulfide formation in an *in vitro* peptide-oxidation assay. We tested both TcpG (Val164Ala) and TcpG (Arg134His/Val164Ala). In this assay, both forms of TcpG catalyze peptide oxidation at the same rate as EcDsbA and above the baseline rate of aerial and nonspecific oxidation observed in the absence of enzyme (Fig. 7). These results suggest that TcpG acts primarily as a disulfide oxidant, like EcDsbA.

4. Discussion

V. cholerae is a dangerous human pathogen that is responsible for outbreaks of cholera, a prevalent and problematic public health issue in developing countries where water sanitation is compromised. TcpG is required to correctly fold ToxR-regulated proteins involved in *V. cholerae* fimbriae maturation and the release of virulence factors (Peek & Taylor, 1992). Inhibiting TcpG activity has therefore been suggested as a means of developing drugs for the treatment of cholera (Hu *et al.*, 1997; Heras *et al.*, 2009). Although TcpG was one of the first DsbA proteins to be described and structurally characterized, its redox properties have not previously been reported. We have performed a comprehensive biochemical investigation of TcpG, showing that it catalyzes insulin reduction more rapidly than EcDsbA, that TcpG and EcDsbA have a similar oxidizing ability and that they both possess a destabilizing active-site disulfide.

The high-resolution TcpG crystal structure model includes both oxidized and reduced forms, so that the two redox forms can be compared in the region of the active site to identify possible reasons for the characteristic destabilizing disulfide of DsbA proteins. The crystal structure reveals that a Cys30 C^{β} methylene H atom is very close to the main-chain O atom of Ser27 (2.3 Å) in the presence of the disulfide. The

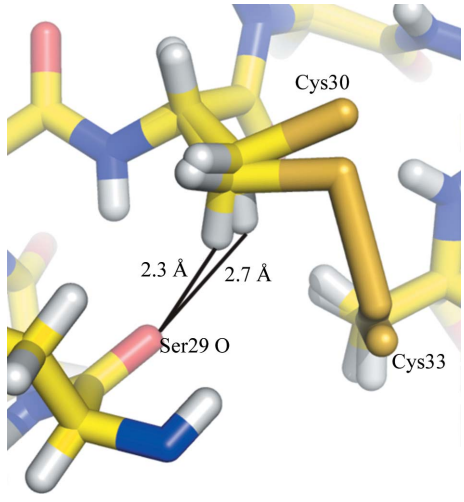

Figure 8
Reduced and oxidized TcpG. The crystal structure of TcpG includes models of both oxidized and reduced TcpG with H atoms included. The presence of a disulfide may cause a steric clash between a methylene H atom of Cys30 and a main-chain O atom of Ser27 (2.3 Å) which is relieved in the reduced structure (2.7 Å).

corresponding distance in the reduced form is 2.7 Å (Fig. 8). The short contact in the oxidized form suggests the possibility of either a C—H···O hydrogen bond (Derewenda *et al.*, 1995) or a steric clash. The contact does not seem to have the appropriate geometry for a C—H···O hydrogen bond, so is probably destabilizing. If so, this contact could contribute to the so-called 'tense' conformation of DsbA proteins (Wunderlich *et al.*, 1993). However, this possible explanation for the destabilizing disulfide requires confirmation by analysis of similarly high-resolution crystal structures (<1.2 Å, with H atoms modelled) of both redox forms of thioredoxin-fold proteins that do not exhibit a destabilizing disulfide (*e.g.* thioredoxin or glutaredoxin). Such structures are currently not available.

The strong insulin-reduction activity of TcpG was unexpected. This prompted us to ask whether *V. cholerae* encodes a DsbC disulfide isomerase homologue. If not, TcpG could potentially catalyse oxidase and isomerase activities. A *BLAST* (Altschul *et al.*, 1990) search of the *Vibrio* B33 genome did identify a potential DsbC homologue (accession code EE_018795). However, the sequence identity of this putative VcDsbC to the *E. coli* disulfide isomerase DsbC was only 21% using *ClustalW* (Thompson *et al.*, 1994). The characteristic sequence motifs of EcDsbC are a CPYC active-site motif (CPHC in EcDsbA) and a Thr preceding the *cis*-Pro loop (Val in EcDsbA). DsbC also forms a V-shaped homodimer (McCarthy *et al.*, 2000) rather than the two-domain monomer of DsbA, which prevents interaction with DsbB (Bader *et al.*, 2001). In all these respects, TcpG is more like EcDsbA than EcDsbC: it interacts with EcDsbB, it does not form a V-shaped homodimer, it has a CPHC active site and a Val-*cis*-Pro motif. We also found that TcpG, unlike DsbC, is able to complement EcDsbA in an *in vivo* motility assay and to catalyze peptide oxidation to the same extent as EcDsbA. Taking these findings into consideration, we conclude that the primary function of TcpG is to catalyze the oxidation of protein cysteines.

We found that reduced TcpG is able to donate its electrons to EcDsbB and thus can be re-oxidized. *V. cholerae* encodes a DsbB (VcDsbB; accession code ZP_01976503) which shares 47% sequence identity with EcDsbB (accession code NP_415703). Similarly, TcpG shares 40% sequence identity with EcDsbA. Interestingly, the periplasmic loop residues of EcDsbB that interact with EcDsbA are highly conserved in the equivalent loop in VcDsbB. Therefore, our finding that TcpG is oxidized by EcDsbB suggests that the mechanism by which TcpG is oxidized *in vivo* will be similar to that of *E. coli*. A model of the EcDsbB and TcpG complex suggests that similar disulfide and hydrogen-bond interactions can occur. However, for the periplasmic loop of DsbB to interact with the TcpG hydrophobic groove in the same way that it interacts with EcDsbA, the TcpG active-site His32 must rotate and the $\beta5$–$\alpha7$ loop must move compared with the conformation observed in the high-resolution crystal structure. Evidence from NMR and proteolysis experiments (Horne *et al.*, 2007) and now crystal structures supports the notion that the $\beta5$–$\alpha7$ loop is flexible, like that of EcDsbA, and therefore it is likely to play the same role in forming part of the binding site of DsbB.

The structural differences between the previously reported crystal structure of TcpG (PDB entry 1bed) and the newly reported crystal structure (PDB entry 4dvc) could be a consequence of the increased resolution of the new TcpG structure, the newer refinement methods used, the different temperatures used for diffraction data measurement, which resulted in a 5% reduction in unit-cell volume for the 1.2 Å resolution structure, the presence of bound small molecules, minor variations in the sequence, the presence of an N-terminal His tag or a combination of these factors. It is likely that we can rule out newer refinement methods, because the *PDB_REDO* structure 1bed_final has much better refinement statistics than 1bed (Table 1) yet shows the same structural differences from 4dvc in the $\beta5$–$\alpha7$ loop and the N-terminus (Supplementary Fig. S3). The structural flexibility at the $\beta5$–$\alpha7$ loop is likely to have a functional role in that it forms part of the proposed DsbB-binding site. By comparison, the N-terminal residues form a relatively unstructured region followed by a β-strand that interacts with $\beta5$, similar to that in EcDsbA. The structural differences observed at the N-terminus for 1bed and 4dvc may therefore simply reflect the variability that is often observed at N- and C-termini.

The lack of surface definition surrounding the TcpG active site in 1bed suggested that identification of small-molecule binders as a starting point for inhibitor design might prove to be difficult. However, the high-resolution TcpG structure identified two potential DMSO-binding sites, one of which is located in the interdomain space between the helical and the thioredoxin domains. This result suggests that it may be possible to discover and design small molecules that target TcpG, opening up the possibility of the development of TcpG inhibitors. Inhibitors of EcDsbB and the related *Mycobacterium tuberculosis* membrane protein VKOR have recently been reported (Früh *et al.*, 2010; Dutton *et al.*, 2010). To date, no inhibitors of DsbA have been described. An inhibitor that targets the region surrounding the active-site disulfide of DsbA could act as a competitive inhibitor of substrate or DsbB binding. An inhibitor that targets the interdomain space might work allosterically by blocking domain-hinge motion: NMR relaxation data for TcpG suggest that such domain motion may support the catalytic cycle (Horne *et al.*, 2007). There is also indirect evidence that allosteric binding to the reverse surface of DsbA can affect redox activity. Thus, the Gram-positive DsbA, BdbD, binds Ca^{2+} on the reverse surface, and allosteric binding of this divalent cation changes the redox potential by 20 mV (Crow *et al.*, 2009).

In conclusion, our investigations have provided a high-resolution structure of TcpG, the *V. cholerae* DsbA and have defined the redox properties and interactions of this enzyme. The inclusion of H atoms in the refined TcpG structure has identified a possible explanation for the tense conformation of oxidized DsbAs, but this requires confirmation using similarly high-resolution pairs of structures from proteins that do not have destabilizing disulfides.

We thank Russell Jarrott for assistance with protein purification, Karl-Fredrik Lindahl for synthesizing UQ1 and Andrew Whitten and Premkumar Lakshmanane for assistance with figures. We are grateful to Tom Caradoc-Davies for his advice on data collection at the Australian Synchrotron. This work was supported by the National Health and Medical Research Council of Australia (NHMRC, Project Grant #455860 to JLM, MJS and BH), an Australian Postgraduate Award to KC, an International Postgraduate Research Scholarship to PW and an ARC Australian Laureate Fellowship (FL0992138) to JLM. JLM is also an Honorary NHMRC Research Fellow (455829).

References

Abramoff, M. D., Magelhaes, P. J. & Ram, S. J. (2004). *Biophotonics Int.* **11**, 36–42.

Afonine, P. V., Mustyakimov, M., Grosse-Kunstleve, R. W., Moriarty, N. W., Langan, P. & Adams, P. D. (2010). *Acta Cryst.* D**66**, 1153–1163.

Altschul, S. F., Gish, W., Miller, W., Myers, E. W. & Lipman, D. J. (1990). *J. Mol. Biol.* **215**, 403–410.

Aslund, F., Berndt, K. D. & Holmgren, A. (1997). *J. Biol. Chem.* **272**, 30780–30786.

Bader, M. W., Hiniker, A., Regeimbal, J., Goldstone, D., Haebel, P. W., Riemer, J., Metcalf, P. & Bardwell, J. C. A. (2001). *EMBO J.* **20**, 1555–1562.

Bader, M., Muse, W., Zander, T. & Bardwell, J. (1998). *J. Biol. Chem.* **273**, 10302–10307.

Bader, M. W., Xie, T., Yu, C.-A. & Bardwell, J. C. A. (2000). *J. Biol. Chem.* **275**, 26082–26088.

Baker, N. A., Sept, D., Joseph, S., Holst, M. J. & McCammon, J. A. (2001). *Proc. Natl Acad. Sci. USA*, **98**, 10037–10041.

Bardwell, J. C. A., Lee, J.-O., Jander, G., Martin, N., Belin, D. & Beckwith, J. (1993). *Proc. Natl Acad. Sci. USA*, **90**, 1038–1042.

Bardwell, J. C. A., McGovern, K. & Beckwith, J. (1991). *Cell*, **67**, 581–589.

Blommel, P. G. & Fox, B. G. (2007). *Protein Expr. Purif.* **55**, 53–68.

Burmeister, W. P. (2000). *Acta Cryst.* D**56**, 328–341.

Chakraborty, S., Mukhopadhyay, A. K., Bhadra, R. K., Ghosh, A. N., Mitra, R., Shimada, T., Yamasaki, S., Faruque, S. M., Takeda, Y., Colwell, R. R. & Nair, G. B. (2000). *Appl. Environ. Microbiol.* **66**, 4022–4028.

Chen, V. B., Arendall, W. B., Headd, J. J., Keedy, D. A., Immormino, R. M., Kapral, G. J., Murray, L. W., Richardson, J. S. & Richardson, D. C. (2010). *Acta Cryst.* D**66**, 12–21.

Chung, C. T. & Miller, R. H. (1988). *Nucleic Acids Res.* **16**, 3580.

Crow, A., Lewin, A., Hecht, O., Carlsson Möller, M., Moore, G. R., Hederstedt, L. & Le Brun, N. E. (2009). *J. Biol. Chem.* **284**, 23719–23733.

Dailey, F. E. & Berg, H. C. (1993). *Proc. Natl Acad. Sci. USA*, **90**, 1043–1047.

DeLano, W. L. (2002). *PyMOL*. http://www.pymol.org.

Derewenda, Z. S., Lee, L. & Derewenda, U. (1995). *J. Mol. Biol.* **252**, 248–262.

Dolinsky, T. J., Czodrowski, P., Li, H., Nielsen, J. E., Jensen, J. H., Klebe, G. & Baker, N. A. (2007). *Nucleic Acids Res.* **35**, W522–W525.

Dolinsky, T. J., Nielsen, J. E., McCammon, J. A. & Baker, N. A. (2004). *Nucleic Acids Res.* **32**, W665–W667.

Dutton, R. J., Wayman, A., Wei, J.-R., Rubin, E. J., Beckwith, J. & Boyd, D. (2010). *Proc. Natl Acad. Sci. USA*, **107**, 297–301.

Emsley, P. & Cowtan, K. (2004). *Acta Cryst.* D**60**, 2126–2132.

Evans, P. (2006). *Acta Cryst.* D**62**, 72–82.

Früh, V., Zhou, Y., Chen, D., Loch, C., Ab, E., Grinkova, Y. N., Verheij, H., Sligar, S. G., Bushweller, J. H. & Siegal, G. (2010). *Chem. Biol.* **17**, 881–891.

Gasteiger, E., Gattiker, A., Hoogland, C., Ivanyi, I., Appel, R. D. & Bairoch, A. (2003). *Nucleic Acids Res.* **31**, 3784–3788.

Gilbert, H. F. (1995). *Methods Enzymol.* **251**, 8–28.

Guddat, L. W., Bardwell, J. C. A., Glockshuber, R., Huber-Wunderlich, M., Zander, T. & Martin, J. L. (1997). *Protein Sci.* **6**, 1893–1900.

Heras, B., Shouldice, S. R., Totsika, M., Scanlon, M. J., Schembri, M. A. & Martin, J. L. (2009). *Nature Rev. Microbiol.* **7**, 215–225.

Holmgren, A. (1979). *J. Biol. Chem.* **254**, 9627–9632.

Horne, J., d'Auvergne, E. J., Coles, M., Velkov, T., Chin, Y., Charman, W. N., Prankerd, R., Gooley, P. R. & Scanlon, M. J. (2007). *J. Mol. Biol.* **371**, 703–716.

Hu, S.-H., Peek, J. A., Rattigan, E., Taylor, R. K. & Martin, J. L. (1997). *J. Mol. Biol.* **268**, 137–146.

Huber-Wunderlich, M. & Glockshuber, R. (1998). *Fold. Des.* **3**, 161–171.

Inaba, K. & Ito, K. (2002). *EMBO J.* **21**, 2646–2654.

Inaba, K., Murakami, S., Suzuki, M., Nakagawa, A., Yamashita, E., Okada, K. & Ito, K. (2006). *Cell*, **127**, 789–801.

Joosten, R. P., Joosten, K., Murshudov, G. N. & Perrakis, A. (2012). *Acta Cryst.* D**68**, 484–496.

Kabsch, W. (2010). *Acta Cryst.* D**66**, 125–132.

Kurz, M., Iturbe-Ormaetxe, I., Jarrott, R., Shouldice, S. R., Wouters, M. A., Frei, P., Glockshuber, R., O'Neill, S. L., Heras, B. & Martin, J. L. (2009). *Antioxid. Redox Signal.* **11**, 1485–1500.

Liang, L. & Fener, C. (2004). *Synth. Commun.* **34**, 4.

Macnab, R. M. (1986). *Methods Enzymol.* **125**, 563–581.

Martin, J. L. (1995). *Structure*, **3**, 245–250.

Martin, J. L., Bardwell, J. C. A. & Kuriyan, J. (1993). *Nature (London)*, **365**, 464–468.

McCarthy, A. A., Haebel, P. W., Törrönen, A., Rybin, V., Baker, E. N. & Metcalf, P. (2000). *Nature Struct. Biol.* **7**, 196–199.

McCoy, A. J., Grosse-Kunstleve, R. W., Adams, P. D., Winn, M. D., Storoni, L. C. & Read, R. J. (2007). *J. Appl. Cryst.* **40**, 658–674.

McPhillips, T. M., McPhillips, S. E., Chiu, H.-J., Cohen, A. E., Deacon, A. M., Ellis, P. J., Garman, E., Gonzalez, A., Sauter, N. K., Phizackerley, R. P., Soltis, S. M. & Kuhn, P. (2002). *J. Synchrotron Rad.* **9**, 401–406.

Nelson, J. W. & Creighton, T. E. (1994). *Biochemistry*, **33**, 5974–5983.

Pace, C. N., Hebert, E. J., Shaw, K. L., Schell, D., Both, V., Krajcikova, D., Sevcik, J., Wilson, K. S., Dauter, Z., Hartley, R. W. & Grimsley, G. R. (1998). *J. Mol. Biol.* **279**, 271–286.

Paxman, J. J., Borg, N. A., Horne, J., Thompson, P. E., Chin, Y., Sharma, P., Simpson, J. S., Wielens, J., Piek, S., Kahler, C. M., Sakellaris, H., Pearce, M., Bottomley, S. P., Rossjohn, J. & Scanlon, M. J. (2009). *J. Biol. Chem.* **284**, 17835–17845.

Peek, J. A. & Taylor, R. K. (1992). *Proc. Natl Acad. Sci. USA*, **89**, 6210–6214.

Peterson, K. M. (2002). *Curr. Issues Intest. Microbiol.* **3**, 29–38.

Roberts, B. R., Wood, Z. A., Jönsson, T. J., Poole, L. B. & Karplus, P. A. (2005). *Protein Sci.* **14**, 2414–2420.

Rozhkova, A., Stirnimann, C. U., Frei, P., Grauschopf, U., Brunisholz, R., Grütter, M. G., Capitani, G. & Glockshuber, R. (2004). *EMBO J.* **23**, 1709–1719.

Shevchik, V. E., Condemine, G. & Robert-Baudouy, J. (1994). *EMBO J.* **13**, 2007–2012.

Shimizu, N., Hirata, K., Hasegawa, K., Ueno, G. & Yamamoto, M. (2007). *J. Synchrotron Rad.* **14**, 4–10.

Shouldice, S. R., Heras, B., Walden, P. M., Totsika, M., Schembri, M. A. & Martin, J. L. (2011). *Antioxid. Redox Signal.* **14**, 1729–1760.

Studier, F. W. (2005). *Protein Expr. Purif.* **41**, 207–234.

Thompson, J. D., Higgins, D. G. & Gibson, T. J. (1994). *Nucleic Acids Res.* **22**, 4673–4680.

Vivian, J. P., Scoullar, J., Rimmer, K., Bushell, S. R., Beddoe, T., Wilce,

M. C., Byres, E., Boyle, T. P., Doak, B., Simpson, J. S., Graham, B., Heras, B., Kahler, C. M., Rossjohn, J. & Scanlon, M. J. (2009). *J. Mol. Biol.* **394**, 931–943.
Winn, M. D. *et al.* (2011). *Acta Cryst.* D**67**, 235–242.
Wunderlich, M., Jaenicke, R. & Glockshuber, R. (1993). *J. Mol. Biol.* **233**, 559–566.